Science of the Total Environment 790 (2021) 148036

Contents lists available at ScienceDirect

Science of the Total Environment

journal homepage: www.elsevier.com/locate/scitotenv

Isotopic content in high mountain karst aquifers as a proxy for climate change impact in Mediterranean zones: The Port del Comte karst aquifer (SE Pyrenees, Catalonia, Spain)

J. Jódar [a,*], I. Herms [b], L.J. Lambán [a], S. Martos-Rosillo [a], C. Herrera-Lameli [c], J. Urrutia [c,d], A. Soler [e], E. Custodio [f]

[a] Geological Institute of Spain (IGME), Spain
[b] Àrea de Recursos Geològics. Institut Cartogràfic i Geològic de Catalunya (ICGC), Barcelona, Spain
[c] Centro de Investigación y Desarrollo de Ecosistemas Hídricos, Universidad Bernardo O'Higgins, Santiago, Chile
[d] HEUMA, Department of Mining Engineering, Universidad de Antofagasta, Antofagasta 2030, Chile
[e] Grup MAiMA, SGR Mineralogia Aplicada, Geoquímica i Geomicrobiologia, Departament de Mineralogia, Petrologia i Geologia Aplicada, Facultat de Ciències de la Terra, Universitat de Barcelona (UB), C/Martí i Franquès s/n, 08028 Barcelona, Spain
[f] Groundwater Hydrology Group, Dept. Civil and Environmental Eng., Technical University of Catalonia (UPC). Royal Academy of Sciences, of Spain

HIGHLIGHTS

- Water resources generated in the Port del Comte aquifer will decrease in the future.
- Future system discharge during both the thaw and the low flows seasons will be lower.
- Multi-model and multi-scenario used to assess isotopic content trends in groundwater.
- The Isotopic content in groundwater ($\delta^{18}O_{GW}$) shows trends statistically significant.
- Trends in $\delta^{18}O_{GW}$ can be used as proxy of Climate Change impact in aquifer systems.

GRAPHICAL ABSTRACT

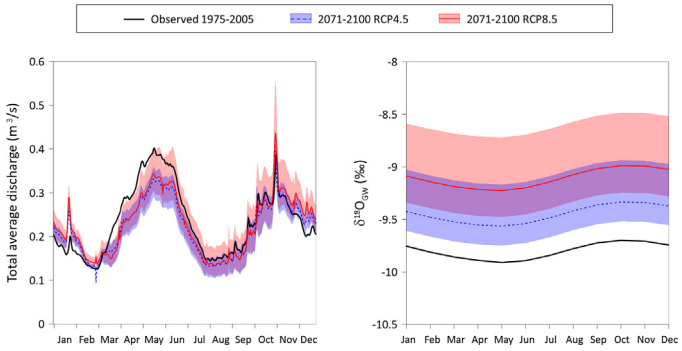

ARTICLE INFO

Article history:
Received 19 April 2021
Received in revised form 18 May 2021
Accepted 21 May 2021
Available online 29 May 2021

Editor: Damia Barcelo

Keywords:
Environmental isotopes
Mountain aquifers
Climate change
Karst

ABSTRACT

The objective of this work is to characterize the impact of climate change in the karst aquifer of the Port del Comte Massif (PCM). Six regional climate models (RCMs) from CLYM'PY Project are used to analyse the magnitude and trends of changes on precipitation and temperature (RCP4.5 and RCP8.5 scenarios) and how these changes propagate through the hydrogeological system as groundwater resources availability and the associated water isotopic content. The study uses the RCMs climate change forcings as input data to a combination of (1) a semi-distributed hydrological model for simulating the hydrodynamical response of the aquifer, and (2) a lumped parameter model for simulating the isotopic content in groundwater at the outlet of the aquifer. A mean decrease of 2.6% and 1.9% in yearly precipitation and a mean increase of 1.9 and 3.1 °C in average temperature is expected in PCM at the end of the 21st century in the RCP4.5 and RCP8.5 scenarios, respectively. This climate signal entering the hydrogeological system results in a mean decrease in recharge of 3.9% and 0.5% from rainfall and of 59.3% and 76.1% from snowmelt, and a decrease of 7.6% and 4.5% in total system discharge, but also generates an isotopic enrichment in groundwater discharge ($\delta^{18}O_{GW}$) of 0.50‰ and 0.84‰, respectively.

* Corresponding author.
E-mail address: j.jodar@igme.es (J. Jódar).

https://doi.org/10.1016/j.scitotenv.2021.148036

Recharge
Trends

Moreover, from a long-term (2010−2100) perspective, the mean trend in $\delta^{18}O_{GW}$ is 0.7‰/100 yr and 1.2‰/100 yr for RCP4.5 and RCP8.5, respectively, resulting in easily measurable annual lapse rates with the current analytical methods.

1. Introduction

High mountain zones are known as "water towers" because they generate the main water resources feeding the downstream depending ecosystems (Viviroli et al., 2007). When mountains constitute an aquifer, the recharged water remains longer in the basin, thus providing a strategic water resource in dry seasons, which is especially important in the drought-prone Mediterranean area (Hoerling et al., 2012; Vicente-Serrano et al., 2014), where water availability is scarce and greatly dependent on runoff from headwater basins (De Jong et al., 2009). In this framework, it is essential to assess the impact of Climate Change (CC) on water resources availability in mountain areas (Chen et al., 2018). This will help to design the most appropriate adaptation measures to minimize adverse effects.

A plethora of climate models have been developed to investigate the extent of CC impact in the future. In their beginning, with no reference solutions available at that time, these models were generally tuned and evaluated against present day conditions. The intercomparison of models has become a mainstream method to assess the uncertainty and robustness of the different climate model predictions (Cess et al., 1989; Gates et al., 1999; Lambert and Boer, 2001; Taylor et al., 2012; Giorgetta et al., 2013; Eyring et al., 2016). A step ahead was done when climate models were used to reproduce the climate of the past, trying to simulate long complex climate scenarios based on proxy climate information (Braconnot et al., 2012; Lohmann et al., 2013; Pfeiffer and Lohmann, 2016). In this line and more recently, paleoclimate modelling studies have begun to adopt a new strategy by using fully coupled isotope-enabled global climate models (IGCM), allowing them to directly simulate paleoclimate proxies (Sjolte and Hoffmann, 2014; Holloway et al., 2016; Gierz et al., 2017; Cauquoin et al., 2019; Sjolte et al., 2020). Nevertheless, all these models require a direct validation using independent isotopic proxy data.

The stable H and O isotopes of water have become a relevant geochemical climate proxy. Their fractionation mechanisms along with their distribution throughout the hydro-climatic system make them a useful tool for reconstructing past climate situations (Dansgaard, 1964). In terms of climate model reliability, it is assumed that the better the model reproduce the paleoclimate evolution the better will perform the model for the future simulated scenarios. However, the paleoclimate reconstructions to be accounted by climate models rely on geochemical proxies to allow for the reconstruction of the climate state in the past, which is a method subject to potential errors and need calibration. For the reconstruction of past climate, a global database of speleothem carbon and oxygen isotope proxy records has been compiled recently, which include 455 records covering intervals within the last 21 ka (Atsawawaranunt et al., 2018, 2019). This information constitutes an "out-of-sample" test to evaluate the climate models against paleorecords for climate reconstruction (Schmidt et al., 2014). Additional information that is currently being used as climate proxy data is the oxygen and hydrogen isotopic content in water from the Global Networks of Isotopes in Precipitation (GNIP) and Rivers (GNIR), which are managed by the International Atomic Energy Agency (IAEA) in cooperation with the World Meteorological Organization (WMO). To complement this, a global analysis, based on oxygen isotope content in modern cave drip water sampled in 163 drip sites, from 39 caves on five continents has been compiled recently (Baker et al., 2019). However, all this information is unevenly distributed, thus with large zones with scarce and even nil spatial coverage for precipitation isotope data, especially in mountain zones.

Carbonated karst aquifers may represent 15.2% of the land surface, of which 68.9% can be found globally in hills and mountain zones (Goldscheider et al., 2020). These aquifers have characteristics that make them quite different from other aquifers, such as high heterogeneity due to the endokarstic network (Bakalowicz, 2005), high velocities of groundwater flow in cavities, and short water residence times (Kiraly, 2003; Motyka, 1998). These hydrodynamic features allow a fast transmission of the recharge inflow signal, including the variation the environmental tracers entering the system with recharge, such as $\delta^{18}O$, to the outflow points draining aquifer. The hydrogeological system filters the high variability and dampens the seasonal variations of the input tracer signal (Jódar et al., 2014, 2016; Herms et al., 2019). This helps to identify in the output tracer signal the mean tracer content and any trend relative to the input tracer signal. Accordingly, the O and H isotopic content of groundwater discharge from karst aquifers can be used as climate proxy data for validating climate models, as those obtained by the GNIP and GNIR programs.

Lumped parameter models (LPMs) are useful to simulate the behaviour of complex mountain karst systems, even when their heterogeneity is poorly characterized (Hartmann et al., 2014). These models do not require a detailed hydrological knowledge of the physical system. Nevertheless, they allow reproducing the observed hydrodynamical response of such aquifers in terms of both, groundwater discharge and the associated tracer content for the corresponding measured input signals (Herms et al., 2019). Moreover, such models transform scenarios of CC into their hydrological results. In this sense, Custodio et al. (2018) analyzed the effect on groundwater reserve and chloride and radiocarbon content of a wetter-than-present period, with enhanced recharge, on data collected from springs in arid lands. In this framework, the evolution in the isotopic content of groundwater for the different simulated scenarios may become a relevant source of isotopic data to be used by IGCMs for validating purposes, as they do currently with paleoclimate proxies such as $\delta^{18}O$ content in ice cores and speleothemes (Gierz et al., 2017; Cauquoin et al., 2019; Sjolte et al., 2020). Surprisingly, there are no references in the scientific literature using either the O and H isotopic content in groundwater nor the expected evolution under CC scenarios as proxy data to validate IGCMs.

Understanding karst aquifer response to changing climate is critical from a water resources perspective, especially in the pan-Mediterranean zone, where water scarcity become a recurrent issue (Pedro-Monzonís et al., 2015). This work aims at characterizing the propagation of the CC impact in the Port del Comte Massif (PCM), a Mediterranean mountain karst aquifer located in the south-eastern sector of the Pyrenees, which plays a strategic role in providing water resources transferred to the metropolitan area of Barcelona. The analysis is focussed on the evolution of (1) the relevant hydrological variables controlling the mass water balance in the aquifer and their impact in the associated water resources, and (2) the isotopic content of the groundwater aquifer discharge, with the aim of identifying relevant trends to be used as CC impact proxies. Although the results of this work are specific for the PCM, the methods, proceedings and the general conclusions can be used in any other mountain karst aquifer.

2. Study area

The study area is located in the massif of Port del Comte (PCM), in the Eastern Pyrenees (Fig. 1). The area is thoroughly described in Herms et al. (2019, 2021). Only a summary describing the most important features is included here. The hydrological basin presents an abrupt

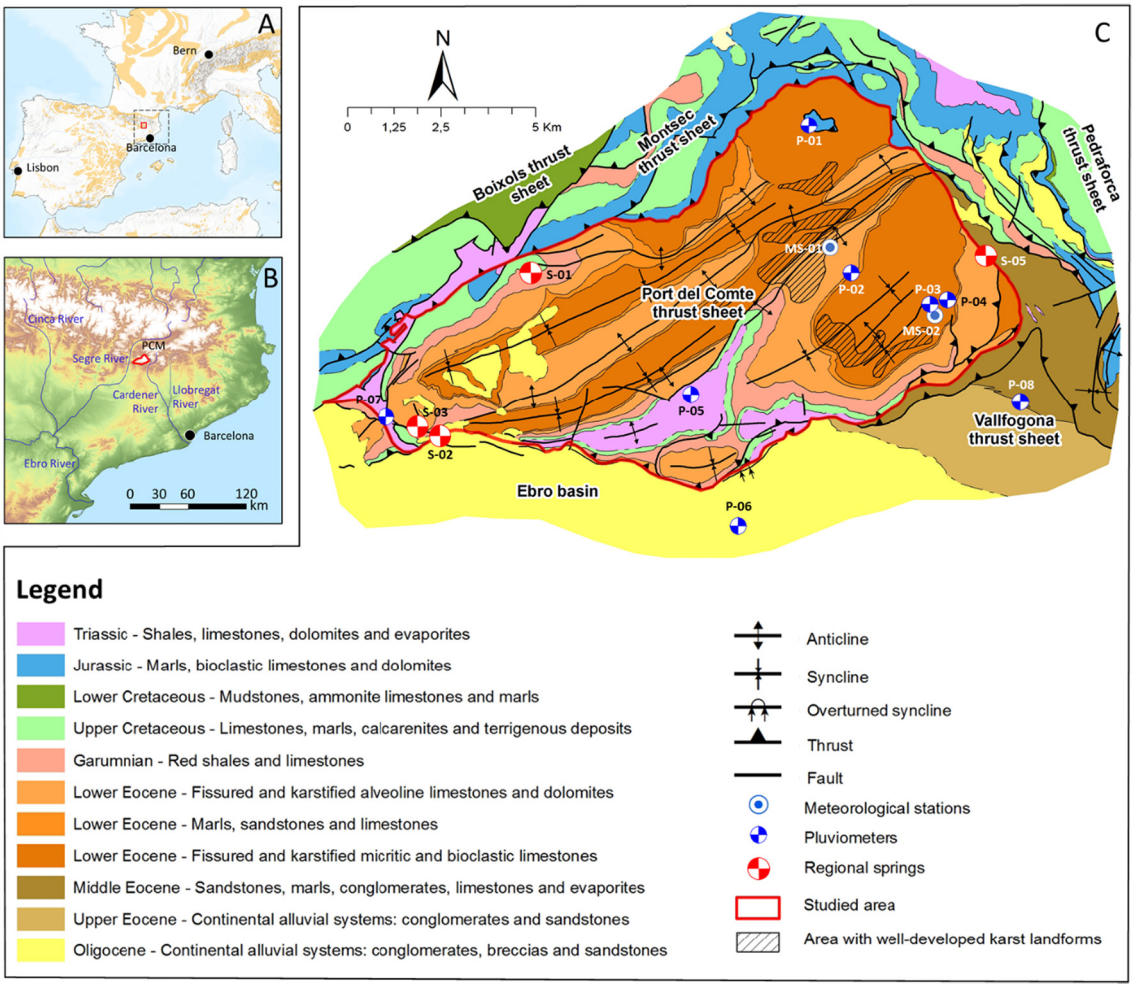

Fig. 1. (A) General map of southern west European continent where the brown shaded areas correspond to carbonate rock outcrops (map modified from the World Map of Carbonate Rock Outcrops v.3.0. (http://www.fos.auckland.ac.nz/our_research/karst). The shaded square shows the limits of the hydrological map shown in the inset below, while the small red square indicates the position of the Port del Comte Massif (PCM). (B) Hydrological setting of PCM (Digital elevation model from "Copernicus Land Monitoring Service", available from https://land.copernicus.eu/imagery-in-situ/eu-dem). (C) Geological map of PCM (modified from Herms et al., 2019). (For interpretation of the references to colour in this figure legend, the reader is referred to the web version of this article.)

topography. The elevation of the massif varies between 900 and 2387 m a.s.l. The PCM has an area of 130 km^2 and separates the Segre and Cardener river basins. The Segre River flows in the N part to the W and then turns to the S at the W side. The Cardener River, the main tributary to the Llobregat River, is at the E side and flows to the S.

From a climatic perspective, and according to the Köppen-Geiger classification, the study area presents a cold climate without a dry season and with cool summers. In the meteorological station MS-02, located at 2315 m a.s.l., precipitation (P), temperature (T) and potential evapotranspiration (PET, Hargreaves and Samani, 1982) show a seasonal variation (Fig. 2) with mean annual values of 1047 mm/yr, 7.0 °C and 525 mm/yr for P, T and PET, respectively. The maximum of precipitation is in autumn, coinciding with the convective thunderstorms typical of the Mediterranean. Precipitation declines in winter to reach the minimum and then increases to reach a second peak in spring. In winter and spring, solid precipitation falls above 1800 m a.s.l.. The snow remains on the slopes and summits of the massif for 3 or 4 months before completely melting. In summer precipitation reaches a second marked minimum.

From a hydrogeological perspective, the carbonate karstified rocks of the Paleocene-Eocene formation hold the main aquifer of the PCM. The massif constitutes an independent structural and hydrogeological unit. Surface runoff is negligible, in agreement with the karstic nature of the massif. Aquifer recharge is produced by the infiltration of water from rainfall and snow melting. The aquifer discharges through a series of springs, of which only four (Fig. 1) have discharge rates greater than 1 L/s. The most important of them is Fonts del Cardener spring (S-05), which has a recharge area of 21.5 km^2, and produces a mean discharge of 7.5 hm^3/yr that tributes downstream into the Llobregat River and amounts 7% of the mean annual water use of Barcelona (Barcelona City Council, 2018).

The mean isotopic content of groundwater discharge in spring S-05 (δ_{GW}) is −9.7‰ and −63.3‰ for $\delta^{18}O$ and $\delta^{2}H$ respectively. These values coincide with the mean isotopic content of precipitation in the spring recharge zone. Moreover, the isotopic content of precipitation (δ_P) shows a seasonal variation, with heavier isotopic compositions in summer and lighter in autumn and winter (Fig. 3A), in agreement with the observed relationship between the isotopic fractionation and temperature (Clark and Fritz, 1997). δ_{GW} follows the sinusoidal variation of δ_P (Fig. 3B), thus indicating the short groundwater mean arrival time of 2.85 yr that has been estimated for this spring (Herms et al., 2019).

3. Methods and materials

The starting point is the combination of the hydrological and the environmental tracer transport models, known here as "hydrological model chain", to reproduce the observed hydrodynamic behaviour of

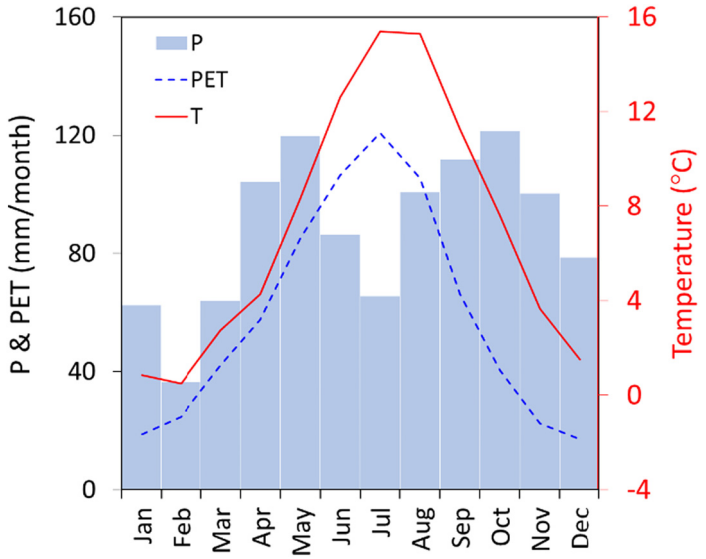

Fig. 2. Average seasonal variation of monthly precipitation (bars), potential evapotranspiration (dashed line) and temperature (line) measured at the meteorological station MS-02 (Fig. 1), located at 1800 m a.s.l., for the period Jan 1990–Sep 2016.

both groundwater discharge and its O and H isotopic content in the PCM aquifer system (Herms et al., 2019).

Next, an ensemble of climate projections is used as input to the calibrated hydrological model to create an ensemble of future recharge values to the aquifer system. To this end, a delta change approach is used to calculate the CC signal between reference and future climate scenarios from precipitation and temperature. The CC signal is then used to modify the observed precipitation and temperature time series and therefore running the hydrological model chain. This allows evaluating the impact of CC on the groundwater system and its O and H isotopic content.

3.1. Hydrological model chain

Numerical lumped models of flow and transport calibrated by Herms et al. (2019) are used in this work to simulate the future hydrological behaviour of PCM.

The hydrodynamic behaviour of the aquifer is simulated in terms of spring discharge with the semi-distributed conceptual precipitation–runoff model HBV-Light (Seibert and Vis, 2012). This model is a standard tool for simulating high mountain snow-dominated hydrological systems (e.g., Konz and Seibert, 2010; Staudinger et al., 2017; Chen et al., 2018; Epting et al., 2018; Jódar et al., 2018; Herms et al., 2019). The HBV model solves a general water balance equation, requiring as input data hydroclimatic daily time series of P, T and PET, and some catchment information including (1) the vertical lapse rates of P and T, and (2) the relative weight with respect to the total catchment area of the different altitude and associated vegetation zones in the basin. For a given day, the model considers precipitation as rain or snow, depending on whether the corresponding daily temperature is above or below a threshold temperature. The snow accumulation and melting are computed according to a degree-day method by a snow routine. A two stacked linear reservoir is used to simulate the hydrological system dynamics. The upper reservoir is used to generate surface and subsurface runoff, and the lower reservoir generates groundwater runoff. As output, model HBV provides the daily basin discharge as the sum of surface and subsurface runoffs, but also provides the daily time series of aquifer recharge, which is afterwards used to simulate the hydrological system response to an environmental tracer input function that enters and migrates through the aquifer from the recharge zones to the discharge springs.

The isotopic content variation in groundwater is simulated with FlowPC (Małoszewski and Zuber, 1996, 2002). FlowPC is a lumped parameter model that requires only a few input parameters. It is useful in alpine catchment areas, where data are often scarce (Małoszewski et al., 1992, 2002; Müller et al., 2013; Lauber and Goldscheider, 2014; Jódar et al., 2016; Herms et al., 2019). The model solves numerically the convolution integral [Eq. (1)] to transform the isotopic input tracer signal $\delta_{in}(t)$ entering the hydrogeological system as recharge into the output tracer signal $\delta_{out}(t)$ leaving the system as spring discharge (Fig. 4).

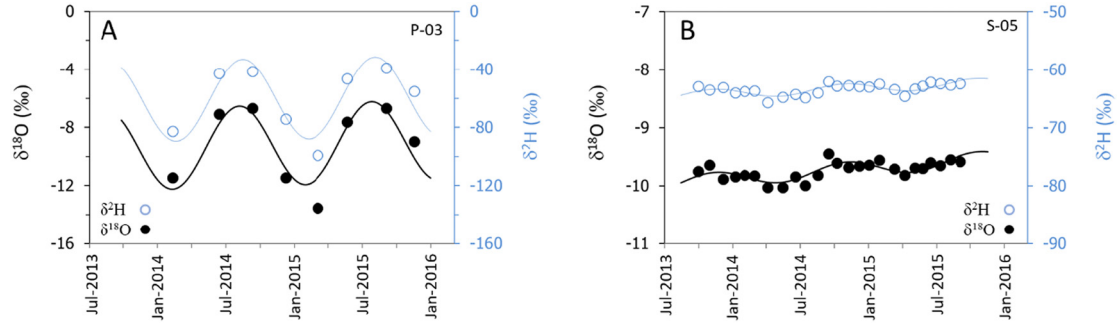

Fig. 3. Seasonal variation of O and H isotopic content. (A) δ_P in precipitation in pluviometer P-03. (B) δ_{GW} in spring S-05. In both cases $\delta^{18}O$ and δ^2H are indicated by solid and empty symbols, respectively. The sinusoidal lines in the figures correspond to the regression fit to the observed δ_P and δ_{GW} data (Jódar et al., 2016). These lines are thick and thin for $\delta^{18}O$ and δ^2H, respectively. The identification codes P-03 and S-05 correspond to those of Fig. 1.

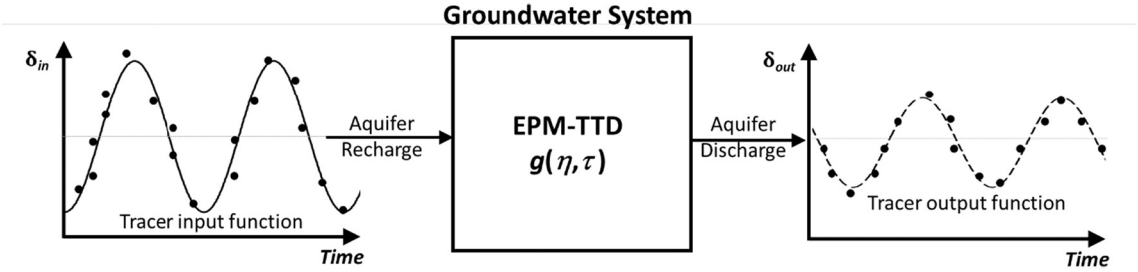

Fig. 4. Schematic representation of the groundwater system response to a hypothetical input tracer function (modified from Jódar et al., 2016).

$$\delta_{out}(t) = \int_{-\infty}^{t} \delta_{in}(t) g(t-\xi) d\xi \quad (1)$$

where t is the time, ξ is the integration variable, g(τ) is a weighting function describing the transit time distribution (TTD) exit of tracer that entered the aquifer at different times in the past, and therefore implicitly includes hydraulic properties of the aquifer, and τ is the system transit time. FlowPC has already implemented four analytic g(τ) functions (Małoszewski and Zuber, 2002). In this work, the exponential piston flow (EPF) TTD is used, as did Herms et al. (2019) to reproduce the observed O and H isotopic content variation in groundwater for the PCM aquifer system. This distribution assumes that the system is composed of two parts in line, one of them with a volume V_{EM} and an exponential distribution of transit times, and the other one with a volume V_{PF} and a piston flow transit time distribution (Zuber, 1986). The parameter $\eta = (V_{EM} + V_{PF})/V_{EM}$, along with τ characterize the EPF-TTD of the system. For spring S-05, the values of η and τ are 1.02 and 2.88 yr, respectively (Herms et al., 2019).

The FlowPC model requires the time series of (1) monthly aquifer recharge, which is obtained by integrating monthly the daily recharge values from HBV, and (2) the monthly averaged isotopic content of recharge ($\widehat{\delta_R}$), which is assumed the same as the monthly averaged isotopic content of precipitation ($\widehat{\delta_P}$), given the karst nature of PCM. This assumption implicitly assumes that the correlation between δ_P and T (Fig. 4) also holds for δ_R and T.

The O and H isotopic signature of rainfall is linked strongly to changes in surface temperature (Dansgaard, 1964; Rozanski et al., 1992), especially in mid latitudinal to high latitudinal regions. This relationship has been used often as a paleothermometer and should be accounted if the climate community aims to better understand possible future warmer-than-present climate scenarios by examining past warm periods. Although this relationship may change in space and time (Gierz et al., 2017), it is known that the temporal slope of the δ_P-T relation has remained largely stable throughout the last 21,000 years over the middle and high latitudes of the globe. In the pan-Mediterranean zone, this temporal slope (m) is about 0.27‰/°C (Guan et al., 2016). The isotopic composition of recharge δ_R for the future scenarios is therefore estimated as

$$\delta_R(T) = m(T-\bar{T}) + T-\overline{\delta_R} \quad (2)$$

where $\bar{T}$ and $\overline{\delta_R}$ are the mean air temperature and isotopic composition recharge for the reference period. For the j-th month of the future climate projection scenario, $\widehat{\delta_{Rj}}$ is obtained by weighting the daily values of recharge isotopic composition δ_{Rij} by the corresponding daily recharge rate Q_{Rij} as

$$\widehat{\delta_{Rj}} = \frac{\sum_{i=1}^{N} \delta_R(T_{ij}) \cdot Q_{R_{ij}}}{\sum_{i=1}^{N} Q_{R_{ij}}} \quad (3)$$

where N is the number of days of the j-th month.

3.2. Delta change approach

A delta change approach (Hay et al., 2000; Räty et al., 2014; Chen et al., 2018) is used to calculate the CC signal between reference and future climate. This signal has been produced specially for the Pyrenees in the framework of the CLYM'PY (Characterization of the evolution of climate and provision of information for adaptation in the Pyrenees) Project (Amblar-Francés et al., 2020), where high–resolution (5 km × 5 km) climate projections for the 21st century have been generated using 24 downscaled general circulation models (GCMs) for several different emission scenarios. This work uses a subset of 6 climate models with the Representative Concentration Pathways (RCP) RCP4.5 and RCP8.5. The former corresponds to a"pathway" in which the radiative forcing stabilizes without overshooting 4.5 W/m^2 (~650 ppm CO_2-equivalent) in 2100, and the latter to the upper bound of the RCPs with a radiative forcing overpassing 8.5 W/m^2 (>1370 ppm CO_2-equivalent) in 2100. In this sense, the term "pathway" stresses that not only the long-term greenhouse gas concentration levels are of interest, but also the trajectory driven along time to reach that outcome (Moss et al., 2010; Van Vuuren et al., 2011).

According to their ability to reproduce the observed climate variability throughout Spain (CEDEX-MAPAMA, 2017), a subset of 6 climate models with the emission scenarios RCP4.5 and RCP8.5 (Table SM1 in Suppl. Mat.) were selected by the Spanish Minister of Agriculture, Fisheries, Food and Environment (MAPAMA) to evaluate the impact of CC on water resources in Spain. The subset includes the following climate models: bcc.csm1.1 (Wu et al., 2014), CNRM.CM5 (Voldoire et al., 2013), inmcm4 (Volodin et al., 2010), MIROC.ESM (Watanabe et al., 2011), MPI.ESM.MR (Giorgetta et al., 2013) and MRI.CGCM3 (Yukimoto et al., 2012). This work adopts this subset as climate model ensemble to assess the impact of CC in the hydrogeological system of PC. In all cases, the temporal period associated to the reference period and future scenarios are 1975–2005 and 2005–2100, respectively.

To simulate the impact of CC in the behaviour of the hydrogeological system, the future model runs (RCM + HBV + FLOWPC) are used to capture the change signal, but not from the raw variables directly (P and T time series from RCMs). For the future period, a delta change approach is used. To this end, synthetic time series of precipitation (P_{sync}) and temperature (T_{sync}) are built based upon their corresponding observed time series (1981–2015), concatenating them in a row, as many times as required, to equal the time interval length comprised in the future simulation scenarios (2005–2100). In this way, the observed seasonal and finer time variability of P and T, which are not captured by the RCMs (Fig. SM1 in Suppl. Mat.), are preserved along with their corresponding frequency-magnitude relationships.

For every RCM, the simulations are used to calculate a multiplicative and an additive correction coefficient (delta change factor), for daily precipitation (P) and temperature (T), respectively, by comparing control and scenario climate model runs, as follows:

$$\alpha(t_i) = \frac{\widetilde{P}(t_i)}{P_{ref}} \quad (4)$$

$$\beta(t_i) = \widetilde{T}(t_i) - T_{ref} \quad (5)$$

where the tilde (~) over the variable stands for the 30 years backward daily mean of the variable for a given day (t_i), and the subscript "ref" stands for the variable averaged value for the last 30 years of the reference period (1975–2005). Once the delta change factors time series are obtained, they are applied to P_{sync} and T_{sync} (Eqs. (6) and (7), respectively; see Fig. SM2 in Suppl. Mat.), thus including the CC signal in the input time series of the hydrological model chain.

$$P(t_i) = \alpha(t_i) \cdot P_{sync}(t_i) \quad (6)$$

$$T(t_i) = \beta(t_i) + T_{sync}(t_i) \quad (7)$$

3.3. Trend analysis of time series

Temporal trends in the isotopic composition are identified using the Mann–Kendall test (MKT). This is a robust test for trend detection, used widely in climatological, hydrological and environmental time series analysis. The test does not assume the data to be distributed according to any rule (e.g., it does not require data to be normally distributed). It is not affected by missing data in the time series other than the fact the number of sample points are reduced and hence might adversely affect the statistical significance. MKT is neither affected by irregular spacing of the time points of measurement nor by the length of the time series.

The MKT statistic S (Mann, 1945; Kendall, 1975) is obtained as

$$S = \sum_{i=1}^{N-1} \sum_{j=i+1}^{N} \operatorname{sgn}(x_i - x_j) \quad (8)$$

where N is the number of data points in the time series, x_i is the i-th data value in the time series, and $\operatorname{sgn}(x_i - x_j)$ is the indicator sign function defined by

$$\operatorname{sgn}(x_i - x_j) = \begin{cases} 1; x_i - x_j > 0 \\ 0; x_i - x_j = 0 \\ -1; x_i - x_j < 0 \end{cases} \quad (9)$$

The variance associated with S is calculated as

$$\sigma_S^2 = \frac{1}{18}\left(N(N-1)(2N+5) - \sum_{k=1}^{h} n_k(n_k-1)(2n_k+5)\right) \quad (10)$$

where h is the total number of tied groups in the data, n_k is the number of ties of extent k. A tied group is a set of sample data having the same value.

For large sample sizes ($N > 10$), S is approximated by the normal distributed statistic Z_S (Eq. (11)), which is used by most statistical software. In this work, the trend analysis has been conducted using both the computer Program of Trend Test from the USGS (Helsel and Frans, 2006; Helsel et al., 2006), and the Real Statistics Resource Pack software (Zaiontz, 2020).

$$Z_S = \begin{cases} (S-1)/\sigma_S; S > 0 \\ 0; S = 0 \\ (S+1)/\sigma_S; S < 0 \end{cases} \quad (11)$$

Positive and negative values of Z_S indicate increasing and decreasing trends, respectively. The trends are tested at a given significance level α. If $|Z_S| > |Z_{1-\alpha/2}|$, then the null hypothesis (i.e., there is no trend) is rejected and a significant trend is assumed in the time series. $Z_{1-\alpha/2}$ is the corresponding value of $P = \alpha/2$ for a standard normal distribution. In this work the significance level of 0.05 is considered. Therefore $Z_{1-\alpha/2} = 1.96$.

The slope of trend β in the time series is evaluated by the non-parametric procedure proposed by Sen (1968). It is calculated by

$$\beta = median\left(\frac{x_j - x_i}{j-i}\right); j > i \quad (12)$$

The confidence interval for the Sen's slope (β_L, β_U) can be computed as (Hollander and Wolfe, 1973; Gilbert, 1987)

$$\beta_L = \frac{1}{2}(N - C_\alpha) \quad (13)$$

$$\beta_U = \frac{1}{2}(N + C_\alpha) \quad (14)$$

$$C_\alpha = \sigma_S \cdot Z_{1-\alpha/2} \quad (15)$$

The MKT is indeed a robust test for trend detection. Nevertheless, it is not well suited for data with periodicities (i.e., seasonal effects) because the functional dependence of S (Eq. (8)). To ensure the effectiveness of MKT for detecting trends, the seasonal effects are eliminated in this work by considering annual time series instead of monthly ones. To this end, the monthly time series of precipitation and aquifer recharge are annually integrated, whereas the monthly time series of temperature and isotopic content in water are annually averaged.

4. Results and discussion

4.1. Effect of climate projections on hydrology

The signal of CC enters the hydrological systems through variations in the terms conditioning the mass water balance in the system. Fig. 5 shows the percentage of change associated to precipitation (P), temperature (T), actual evapotranspiration (AET), total runoff (Q_{tot}), rainfall recharge (Q_{rain}), snowmelt recharge (Q_{snow}) and total recharge (Q_{rec}), averaged for the 2011–2040, 2041–2070 and 2071–2100 intervals for the average ensemble of climate models. The interval length has been selected to ensure that the estimated values for the interval are not conditioned by the short-term patterns of temporal variability which often contain the climatic variables.

Precipitation seems to follow a slight downward trend for the different average intervals considered (Fig. 5), presenting maximum annual decreases of 29 and 30 mm for the RCP4.5 and RCP8.5 scenarios, respectively (Table SM2 in Suppl. Mat.). As can be shown, the variability in rainfall for the model ensemble is always greater in the case of the emission scenario RCP8.5. The precipitation signal, including the trend, propagates throughout the hydrological system. It is reflected almost homothetically in the obtained variations of Q_{rain}, Q_{rec} and Q_{tot}. Despite the variations shown for the selected multidecadal intervals, none of these variables present a statistically significant trend for the whole estimation period 2010–2100 (Table 1).

Temperature shows a monotonous increasing trend for the three selected intervals, being the variation greater in every case for the RCP8.5 emission scenario. For the last interval (2071–2100), the average temperature with respect the reference period (1986–2015) is 1.9 and 3.1 °C for the scenarios RCP4.5 and RCP8.5, respectively. The temperature evolution signal propagates in a natural way to both AET and Q_{snw}, as it is well-known that both variables show a large dependence on T. Furthermore, for the whole period 2010–2100, the estimated trends for T, AET and Q_{snw} are statistically significant, increasing for T and AET and decreasing for Q_{snw}, as expectable for a warmer climate scenario. Such decreasing trends in Q_{snw} have been already observed in the Western Pyrenees and other mountain zones (López-Moreno et al., 2009, 2020; Matiu et al., 2021), and are expected to be more marked in the future, especially at low elevations, with more uncertain trends in observations and in future projections at higher elevations (Gobiet et al., 2014; Beniston et al., 2018; Hock et al., 2019; IPCC, 2019).

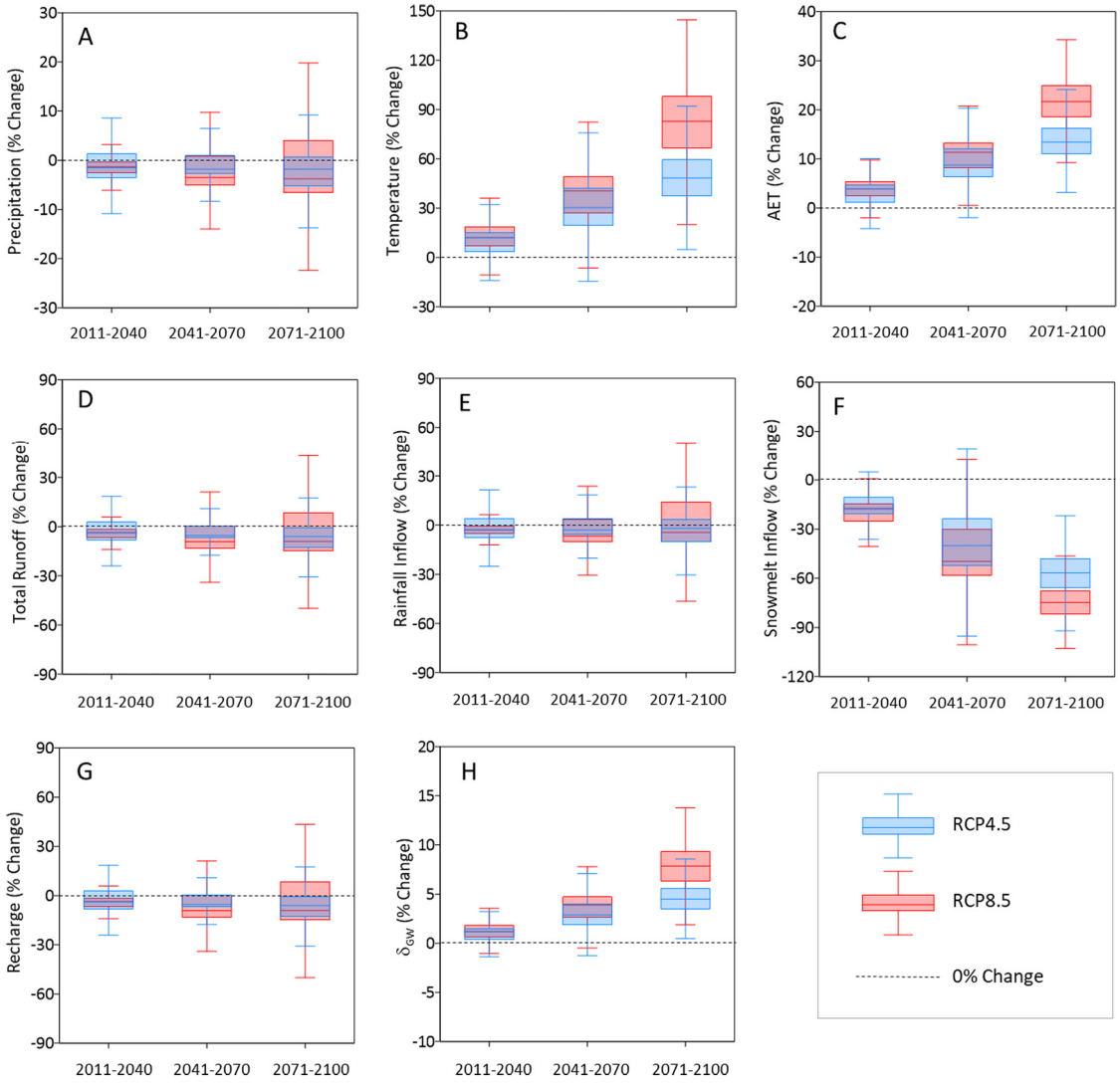

Fig. 5. Percentage of change of the hydrometeorological variables for the averaging periods 2011–2040, 2041–2070 and 2071–2100, obtained by the different climate models for the emission scenarios RCP4.5 and RCP8.5, with respect the corresponding averaged value of the variable obtained for the reference period (1998–2005). The dashed line indicates the null change position.

Previous works focusing on CC impacts in mountain zones indicate a generalized water resources decrease (Beniston and Stoffel, 2014; Beniston et al., 2018). This trend has already been observed in the Pyrenees (López-Moreno et al., 2008b), highlighting the importance of this mountain range as an early warning system to mitigate the impact of CC, among other impacts, by implementing adaptation strategies before the impact arrival in the central and northern European zones. In the case of PCM, climate models predict a slight decrease in the total discharge flow Q_{tot}, with a not statistically significant long-term trend.

The evolution of Q_{tot} is highly controlled by the evolution of P. However, T also plays an important role in this regard, modifying not so much the magnitude of Q_{tot} but the associated seasonality, especially in basins where the dynamics of snow accumulation and melting processes are relevant. Snow melting is a process that maximizes the diffuse recharge of the aquifer, being able to play an important role in the total aquifer recharge if the snow accumulation during the cold season is important, as occurs in the central zone of the Pyrenees (Jódar et al., 2020). Moreover, the snow accumulation and melting diffuse recharge may even condition the speleogenesis and development of karst (González-Ramón et al., 2020). In the study area, the aquifer recharge from snow melt represents only 7% of total recharge. Despite of that, it is enough to leave a clear fingerprint in terms of Q_{tot} response, as revealed when the hydrograph of the reference period is compared with that of the last considered period 2071–2100 (Fig. 6). The latter presents a discharge increase in the winter months (Nov-Feb). This discharge increment is generated by a decrease of snowfall and an increase of rainfall, driven by the warmer climate conditions obtained for the climate models for this period. Consequently, Q_{tot} presents a decrease in the thaw season (Mar-May), as in winter there is less accumulation of snow and therefore a lower snowmelt flow contributing to the total basin discharge in the spring season. In addition, the snow accumulation decrease will reduce the aquifer recharge, thus favoring an earlier low flow season. This effect has been already observed in some high mountain basins (López-Moreno and García-Ruiz, 2004, López-Moreno et al., 2008a, 2008b; Birsan et al., 2005; Bard et al., 2015; Mallucci et al., 2019).

There is a net decrease in the mean annual spring discharge for the third period 2071–2100, of 0.6 and 0.4 hm^3/yr for the emission scenarios RCP4.5 and RCP8.5, respectively. These values may look not a huge decrease, but such variations may be critical downstream for the depending ecosystems (Goldscheider, 2019). These ecosystems are tacking with a structural water scarcity derived from the increased frequency and severity of the current Mediterranean droughts (Hoerling et al., 2012; Vicente-Serrano et al., 2014), and their expected increasing trend in the framework of CC (Cramer et al., 2018).

Table 1
Estimated Sen's slopes for the hydrometeorological variables for the period 2010–2100, considering the different climate models and the two emission scenarios. The blue shaded values indicate statistically significant trends for the whole period.

RCP	GCM	β_P $\left(\frac{mm}{100\ yr}\right)$	β_T $\left(\frac{°C}{100\ yr}\right)$	β_{AET} $\left(\frac{mm}{100\ yr}\right)$	β_R $\left(\frac{mm}{100\ yr}\right)$	$\beta_{Q_{rain}}$ $\left(\frac{mm}{100\ yr}\right)$	$\beta_{Q_{snw}}$ $\left(\frac{mm}{100\ yr}\right)$	$\beta_{Q_{tot}}$ $\left(\frac{mm}{100\ yr}\right)$	$\beta_{\delta^{18}O_P}$ $\left(\frac{‰}{100\ yr}\right)$	$\beta_{\delta^{18}O_{GW}}$ $\left(\frac{‰}{100\ yr}\right)$
4.5	bcc.csm1.1	30.8	2.0	66.9	-2.8	15.4	-10.3	4.0	0.6	0.6
4.5	CNRM.CM5	51.7	1.8	61.3	10.0	31.2	-9.1	17.7	0.5	0.5
4.5	inmcm4	-1.3	1.6	57.3	-27.1	-5.2	-9.0	-19.2	0.5	0.4
4.5	MIROC.ESM	-48.7	4.0	122.3	-54.4	-22.1	-14.5	-46.7	1.1	1.2
4.5	MPI.ESM.MR	-3.2	2.3	76.2	-25.0	2.4	-12.1	-19.0	0.6	0.7
4.5	MRI.CGCM3	-11.6	1.9	68.4	-37.6	-9.7	-11.6	-30.8	0.5	0.5
4.5	*Average*	-9.4	2.3	74.3	-28.9	-3.5	-11.3	-20.8	0.6	0.7
8.5	bcc.csm1.1	-12.9	4.2	128.9	-21.3	5.6	-15.5	-13.9	1.2	1.1
8.5	CNRM.CM5	87.4	3.6	120.7	47.1	76.1	-15.2	54.1	1.0	1.0
8.5	inmcm4	-1.0	3.1	102.4	-28.6	-1.9	-15.1	-24.3	0.9	0.8
8.5	MIROC.ESM	-48.4	7.0	197.2	-46.3	-16.1	-18.0	-43.6	1.9	1.9
8.5	MPI.ESM.MR	-46.1	4.8	145.9	-48.3	-12.8	-17.9	-37.8	1.3	1.3
8.5	MRI.CGCM3	156.0	3.6	126.1	94.0	116.5	-16.2	100.5	1.0	1.0
8.5	*Average*	15.5	4.4	136.6	-2.8	26.6	-16.6	5.0	1.2	1.2

4.2. Effect of climate projections on the isotopic content of groundwater

Meteoric water recharging the aquifer introduces in the system not only the input signal in terms of inflows, but also enters the signal associated to the isotopic content of recharge water. This signal propagates downgradient from aquifer recharge to discharge areas, where regional springs drain the system. In the case of a trending input tracer signal, the trend will be transferred to the output tracer signal unless the tracer was not conservative (Jódar et al., 2014). Additionally, the aquifer filters the high-frequency variability of the input tracer signal, even damping

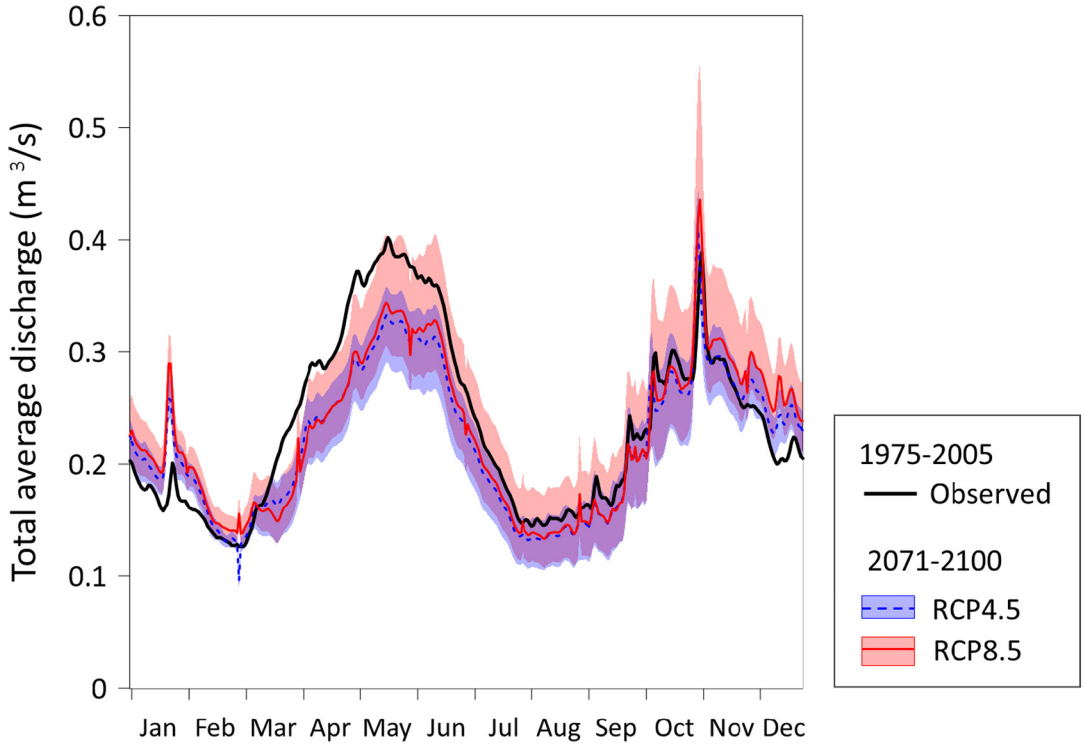

Fig. 6. Seasonal variation of the monthly averaged discharge for both the historical (1986–2015) and future (2071–2100) periods considering the climate projections RCP4.5 and RCP8.5. Black thick line shows Q_{tot} for the reference period. Red line and shaded area indicate mean Q_{tot} and the corresponding variation interval for RCP8.5, whereas blue dashed line and shaded area indicate the mean Q_{tot} and the associated variation interval for RCP4.5. (For interpretation of the references to colour in this figure legend, the reader is referred to the web version of this article.)

the amplitude of the seasonal variation of δ_P (Figs. 3 and 4) (Herms et al., 2019; Jódar et al., 2016, 2020). Such filtering makes it easier identifying trends in the δ_{GW} outflow signal because the "noise" associated to the high frequency variability of δ_P in the inflow signal hinders the trend detection (Fig. SM3 in Suppl. Mat.). In this line, the PCM is an ideal system to evaluate how the signal of the impact of CC is propagated through a karst aquifer. The groundwater mean arrival time of 2.83 yr is long enough to eliminate the high-frequency variability signal of δ_P, but short enough to identify the most significant recharge events at the spring discharge from both the hydrodynamic and the isotopic perspective (Herms et al., 2019).

The evolution of δ_{GW} in spring S-05 shows a trend like that of T, becoming isotopically heavier in an increasing monotonic way for the three intervals considered (Fig. 5). These variations are larger for scenario RCP8.5, regardless of the selected time interval. For the last analyzed period of the 21st century, the average annual increase in δ_{GW} for scenarios RCP4.5 and RCP8.5 is 0.50‰ and 0.84‰, respectively. From a long-term perspective (i.e., 2010–2100; Fig. 7), δ_{GW} shows statistically significant trends of 0.7‰/100 yr and 1.2‰/100 yr RCP4.5 and RCP8.5, respectively (Table 1).

Isotopic information from groundwater ultimately occurs from precipitation, but reflects the interplay between physical aspects of climate, meteorology and geo-hydrology at different spatial-temporal scales. Despite of that, the isotopic content of groundwater reveals as a useful source of information. The hydrogeological systems provide a response in terms of δ_{GW} that reflect faithfully not only the mean value of δ_P but also the associated trends. This behaviour makes the hydrogeological systems especially well-suited to be used as proxy data providers of δ_P for fully IGCM, which is a current promising research line (Yoshimura, 2015).

IGCMs provide the isotopic signal distribution of a particular time period along with the corresponding evolution of climate variables, which is particularly useful in paleoclimate and paleo-altimetry studies (Rowley and Garzione, 2007; Bershaw et al., 2012; Gierz et al., 2017; Cauquoin et al., 2019). Besides, these models unravel the complex relationships between geochemical climate proxies (e.g., ice core $\delta^{18}O$, tree cellulose $\delta^{18}O$, and coral $\delta^{18}O$) and climate simulations (Okazaki and Yoshimura, 2019). To illustrate this, it could be considered to simulate the temperature evolution during interglacial $\delta^{18}O$-climate reconstructions while minimizing possible misinterpretations of isotope records used in such paleo-climatological studies. This is a focal topic given the growing concerns about future global CC. Nevertheless, there is still enough room for improving IGCMs (Gierz et al., 2017). In this regard, there is limited O and H water isotopic data regarding (1) the hydrological processes moving the water vapor in and out of clouds - this is being improved by applying laser spectroscopic isotopic measurement techniques (Wassenaar et al., 2018; Denisova et al., 2020) - and (2) terrestrial hydrological cycles at different scales, including the partitioning of total water transport as surface water, in transit recharge through the vadose zone and groundwater (Yoshimura, 2015). This point may be addressed by adding isotopic content data of both surface water and groundwater, which is crucial information to evaluate averages of precipitation O and H isotope contents at the corresponding aquifer recharge areas, especially in zones with nil spatial coverage of precipitation isotope data. As a result, more certain local and global budget of O and H isotopes could be obtained, especially for groundwater (Henderson-Sellers et al., 2004; Custodio and Jódar, 2016; Baker et al., 2019; Herms et al., 2019) to help validating IGCMs. In this line, the results obtained in this work will be useful to provide plausible scenarios to compare with, while making the IGCMs CC simulations more reliable. This is of paramount importance to develop CC adaptation strategies scaled to the expected impact in the hydrogeological systems.

Karst aquifers have been shown to be very vulnerable, especially to pollution, due to their high hydraulic conductivity and limited self-depuration capacity (Parise et al., 2015). Moreover, when the karst aquifers are unconfined, focused recharge through the most conductive karst features facilitates the widespread rapid incorporation and transport of pollutants to the groundwater (Hartmann et al., 2021). In this framework, and from the perspective of climate change impact, their vulnerability is even higher. In high mountain karst aquifers, the snow cover provides additional water storage for the hydrological system while protecting the aquifer from external pollutants. Besides, in the warm season, the generated snowmelt drives aquifer recharge as a spatially diffuse process driven by the snowmelt infiltration (Meeks and Hunkeler, 2015; Jódar et al., 2020). The snowmelt flows diffusely through the snowpack while maintaining moderate drainage rates. This maximizes infiltration through the uppermost soil/epikarst layer along the slopes of the mountain (Custodio and Jódar, 2016). The warming trends obtained in this work impact directly in the snowpack cover formation and the corresponding snowmelt infiltration (Fig. 5 and

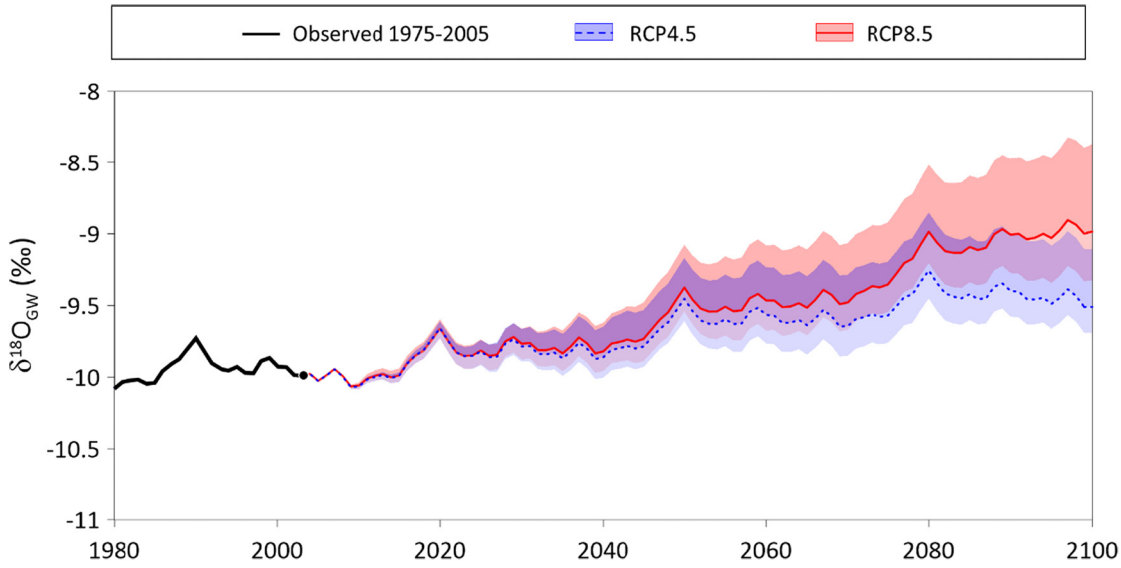

Fig. 7. Evolution of the isotopic ($\delta^{18}O$) content in groundwater discharge for spring S-05 considering the climate projections RCP4.5 and RCP8.5. Black thick line shows δ_{GW} for the reference period. The point marks the beginning of the RCP scenarios. The red line and shaded area indicate mean δ_{GW} and corresponding variation interval for scenario RCP8.5, whereas blue dashed line and shaded area indicate mean δ_{GW} and associated variation interval for scenario RCP4.5 (the violet colored strip is just the overlapping of red and blue). (For interpretation of the references to colour in this figure legend, the reader is referred to the web version of this article.)

Table 1). As a result, the vulnerability of the karst system will be even increased, given that these mountain karst aquifers will be directly exposed longer to eventual contaminant surface spills. As shown, this stresses the interplay between vulnerability to pollutants and impact of climate change, given that they are not independent in high mountain aquifer karst systems.

5. Conclusions

Karst aquifers are particularly vulnerable to the impact of CC because they typically show short transit times that allow a fast propagation of the CC generated hydro- climatical signal through the hydrogeological system. This is the case of the PCM, in which the climate input signal variations propagate quickly through the hydrological system, as reflected in the hydrological variables that control the hydrodynamic functioning of the aquifer and impact the ecosystems dependent on groundwater discharge in a short time.

The estimated evolution of P and T for the last 30 years period of the 21st century shows a net decrease in P and an increase in T. These variations, which regardless of the climate model are bolded in the scenario RCP8.5, are primarily reflected in a decrease of snowfall and snow accumulation, which in turn have immediate consequences on the hydrological system, such as reducing both springtime high flows and aquifer recharge, and advancing the low flows period.

The temporal variability associated to the hydrological variables may hinder the fast detection of CC impact in hydrological systems. Nevertheless, the trend on the isotopic composition of groundwater may be used as a proxy of such impact. In the PCM, the isotopic composition of groundwater shows a clear enrichment trend, with mean rates of 0.7‰/100 yr and 1.2‰/100 yr for scenarios RCP4.5 and RCP8.5, respectively. These values are high enough to produce in the short-mean term an isotopic enrichment in groundwater that are easily detected by available analytical methods. The methodology applied to obtain these values may be applied in other hydrogeological systems to provide valuable information for helping the validation of fully coupled isotope-enabled global climate models. Besides, measuring the evolution of the isotopic composition of groundwater in a regular scheme may serve as prognosis of the CC impact on the sampled aquifer if any isotopic enrichment trend is detected in the mean isotopic composition of the spring discharge.

CRediT authorship contribution statement

J. Jódar: Conceptualization, Resources, Data curation, Visualization, Formal analysis, Writing – original draft, Writing – review & editing. **I. Herms:** Resources, Data curation, Visualization, Writing – original draft, Writing – review & editing. **L.J. Lambán:** Funding acquisition, Project administration, Supervision, Writing – original draft. **S. Martos-Rosillo:** Writing – original draft. **C. Herrera-Lameli:** Writing – original draft. **J. Urrutia:** Writing – original draft. **A. Soler:** Writing – original draft. **E. Custodio:** Formal analysis, Writing – original draft, Writing – review & editing.

Declaration of competing interest

The authors declare that they have no known competing financial interests or personal relationships that could have appeared to influence the work reported in this paper.

Acknowledgments

This research was supported by the projects: PIRAGUA (EFA210/16/PIRAGUA) funded by the European Union through the Interreg-POCTEFA territorial cooperation program; PACE-ISOTEC (CGL2017-87216-C4-1-R) funded by Agencia Estatal de Investigación (AEI) from the Spanish Government and the European Regional Development Fund (FEDER) from EU; and MAG (Mineralogia Aplicada, Geoquimica i Geomicrobiologia, 2017SGR-1733) of the Universitat de Barcelona (UB) funded by the Catalan Goverment (Generalitat de Catalunya). The Spanish Meteorological Agency (AEMET) and the Meteorological Service of Catalonia (SMC) have provided meteorological data. We would also like to thank the anonymous reviewers for their constructive comments and suggestions which led to a substantial improvement of the paper.

Appendix A. Supplementary data

Supplementary data to this article can be found online at https://doi.org/10.1016/j.scitotenv.2021.148036.

References

Amblar-Francés, M.P., Ramos-Calzado, P., Sanchis-Lladó, J., Hernanz-Lázaro, A., Peral-García, M.C., Navascués, B., Domínguez-Alonso, M., Pastor-Saavedra, M.A., Rodríguez-Camino, E., 2020. High resolution climate change projections for the Pyrenees region. Adv. Sci. Res. 17, 191–208. https://doi.org/10.5194/asr-17-191-2020.

Atsawawaranunt, K., Comas-Bru, L., Amirnezhad Mozhdehi, S., Deininger, M., Harrison, S.P., Baker, A., Boyd, M., Kaushal, N., Ahmad, S.M., Ait Brahim, Y., Arienzo, M., Bajo, P., Braun, K., Burstyn, Y., Chawchai, S., Duan, W., Hatvani, I.G., Hu, J., Kern, Z., Labuhn, I., Lachniet, M., Lechleitner, F.A., Lorrey, A., Pérez-Mejías, C., Pickering, R., Scroxton, N., SISAL Working Group Members, 2018. The SISAL database: a global resource to document oxygen and carbon isotope records from speleothems. Earth Syst. Sci. Data 10, 1687–1713. https://doi.org/10.5194/essd-10-1687-2018.

Atsawawaranunt, K., Harrison, S., Comas-Bru, L., 2019. SISAL (Speleothem Isotopes Synthesis and AnaLysis Working Group) database version 1b. University of Reading. Dataset. https://doi.org/10.17864/1947.189.

Bakalowicz, M., 2005. Karst groundwater: a challenge for new resources. Hydrogeol. J. 13, 148–160. https://doi.org/10.1007/s10040-004-0402-9.

Baker, A., Hartmann, A., Duan, W., Hankin, S., Comas-Bru, L., Cuthbert, M.O., Treble, P.C., Banner, J., Genty, D., Baldini, L.M., Bartolomé, M., Moreno, A., Pérez-Mejías, C., Werner, M., 2019. Global analysis reveals climatic controls on the oxygen isotope composition of cave drip water. Nat. Commun. 10 (1), 1–7. https://doi.org/10.1038/s41467-019-11027-w.

Barcelona City Council, 2018. Evolution of water consumption in the city of Barcelona. https://www.bcn.cat/estadistica/angles/dades/economia/consum/evoconsum/coev04.htm.

Bard, A., Renard, B., Lang, M., Giuntoli, I., Korck, J., Koboltschnig, G., Janža, M., d- Amico, M., Volken, D., 2015. Trends in the hydrologic regime of alpine rivers. J. Hydrol. 529, 1823–1837. https://doi.org/10.1016/j.jhydrol.2015.07.052.

Beniston, M., Stoffel, M., 2014. Assessing the impacts of climatic change on mountain water resources. Sci. Total Environ. 493, 1129–1137. https://doi.org/10.1016/j.scitotenv.2013.11.122.

Beniston, M., Farinotti, D., Stoffel, M., Andreassen, L.M., Coppola, E., Eckert, N., Fantini, A., Giacona, F., Hauck, C., Huss, M., Huwald, H., Lehning, M., López-Moreno, J.I., Magnusson, J., Marty, C., Morán-Tejéda, E., Morin, S., Naaim, M., Provenzale, A., Rabatel, A., Six, D., Stötter, J., Strasser, U., Terzago, S., Vincent, C., 2018. The European mountain cryosphere: a review of its current state, trends, and future challenges. Cryosphere 12, 759–794. https://doi.org/10.5194/tc-12-759-2018.

Bershaw, J., Penny, S.M., Garzione, C.N., 2012. Stable isotopes of modern water across the Himalaya and eastern Tibetan Plateau: implications for estimates of paleoelevation and paleoclimate. J. Geophys. Res. Atmos. 117(D2. https://doi.org/10.1029/2011JD016132.

Birsan, M.V., Molnar, P., Burlando, P., Pfaundler, M., 2005. Streamflow trends in Switzerland. J. Hydrol. 314 (1), 312–329. https://doi.org/10.1016/j.jhydrol.2005.06.008.

Braconnot, P., Harrison, S.P., Kageyama, M., Bartlein, P.J., Masson-Delmotte, V., Abe-Ouchi, A., Otto-Bliesner, B.L., Zhao, Y., 2012. Evaluation of climate models using palaeoclimatic data. Nat. Clim. Chang. 2 (6), 417–424. https://doi.org/10.1038/nclimate1456.

Cauquoin, A., Werner, M., Lohmann, G., 2019. Water isotopes–climate relationships for the mid-Holocene and preindustrial period simulated with an isotope-enabled version of MPI-ESM. Clim. Past 15 (6), 1913–1937. https://doi.org/10.5194/cp-2019-72.

CEDEX-MAPAMA, 2017. Evaluación del impacto del cambio climático en los recursos hídricos y sequías en España. Informe Final. Clave CEDEX: 42-415-0-001. Madrid. https://www.miteco.gob.es/es/cambio-climatico/temas/impactos-vulnerabilidad-y-adaptacion/plan-nacional-adaptacion-cambio-climatico/rec_hidricos.aspx.

Cess, R.D., Potter, G.L., Blanchet, J.P., Boer, G.J., Ghan, S.J., Kiehl, J.T., Le Treut, H., Li, Z.X., Liang, X.Z., Mitchell, J.F.B., Morcrette, J.J., Randall, D.A., Riches, M.R., Roeckner, E., Schlese, U., Slingo, A., Taylor, K.E., Washington, W.M., Wetherald, R.T., Yagai, I., 1989. Interpretation of cloud-climate feedback as produced by atmospheric general circulation models. Science 245, 513–516. https://doi.org/10.1126/science.245.4917.513.

Chen, Z., Hartmann, A., Wagener, T., Goldscheider, N., 2018. Dynamics of water fluxes and storages in an Alpine karst catchment under current and potential future climate conditions. Hydrol. Earth Syst. Sci. 22 (7), 3807–3823. https://doi.org/10.5194/hess-22-3807-2018.

Clark, I.D., Fritz, P., 1997. Environmental Isotopes in Hydrogeology. Lewis Publishers, New York.

Cramer, W., Guiot, J., Fader, M., Garrabou, J., Gattuso, J.P., Iglesias, A., Lange, M.A., Lionello, P., Llasat, M.C., Paz, S., Peñuelas, J., Snoussi, M., Toreti, A., Tsimplis, M.N., Xoplaki, E.,

2018. Climate change and interconnected risks to sustainable development in the Mediterranean. Nat. Clim. Chang. 8 (11), 972–980. https://doi.org/10.1038/s41558-018-0299-2.
Custodio, E., Jódar, J., 2016. Simple solutions for steady-state diffuse recharge evaluation in sloping homogeneous unconfined aquifers by means of atmospheric tracers. J. Hydrol. https://doi.org/10.1016/j.jhydrol.2016.06.035.
Custodio, E., Jódar, J., Herrera, C., Custodio-Ayala, J., Medina, A., 2018. Changes in groundwater reserves and radiocarbon and chloride content due to a wet period intercalated in an arid climate sequence in a large unconfined aquifer. J. Hydrol. 556, 427–437. https://doi.org/10.1016/j.jhydrol.2017.11.035.
Dansgaard, W., 1964. Stable isotopes in precipitation. Tellus 16 (4), 436–468. https://doi.org/10.1111/j.2153-3490.1964.tb00181.x.
De Jong, C., Lawler, D., Essery, R., 2009. Mountain hydroclimatology and snow seasonality and hydrological change in mountain environments. Hydrol. Process. 23, 955–961. https://doi.org/10.1002/hyp.7193.
Denisova, N.Y., Gribanov, K.G., Werner, M., 2020. Validation of ECHAM AGCMs using laser spectrometer data from two Arctic stations. Atmos. Ocean Opt. 33, 702–707. https://doi.org/10.1134/S1024856020060093.
Epting, J.M., Page, R., Auckenthaler, A., Huggenberger, P., 2018. Process-based monitoring and modeling of Karst springs – linking intrinsic to specific vulnerability. Sci. Total Environ. 625, 403–415. https://doi.org/10.1016/j.scitotenv.2017.12.272.
Eyring, V., Bony, S., Meehl, G.A., Senior, C.A., Stevens, B., Stouffer, R.J., Taylor, K.E., 2016. Overview of the Coupled Model Intercomparison Project Phase 6 (CMIP6) experimental design and organization. Geosci. Model Dev. 9 (5), 1937–1958. https://doi.org/10.5194/gmd-9-1937-2016.
Gates, W.L., Boyle, J.S., Covey, C., Dease, C.G., Doutriaux, C.M., Drach, R.S., Fiorino, M., Gleckler, P.J., Hnilo, J.J., Marlais, S.M., Phillips, T.J., Potter, G.L., Santer, B.D., Sperber, K.R., Taylor, K.E., Williams, D.N., 1999. An overview of the results of the Atmospheric Model Intercomparison Project (AMIP I). Bull. Am. Meteorol. Soc. 80 (1), 29–56. https://doi.org/10.1175/1520-0477(1999)080<0029:AOOTRO>2.0.CO;2.
Gierz, P., Werner, M., Lohmann, G., 2017. Simulating climate and stable water isotopes during the Last Interglacial using a coupled climate-isotope model. J. Adv. Model. Earth Syst. 9 (5), 2027–2045. https://doi.org/10.1002/2017MS001056.
Gilbert, R.O., 1987. Statistical Methods for Environmental Pollution Monitoring. John Wiley & Sons, New York.
Giorgetta, M.A., Jungclaus, J., Reick, C.H., Legutke, S., Bader, J., Böttinger, M., Brovkin, V., Crueger, T., Esch, M., Fieg, K., Glushak, K., Gayler, V., Haak, H., Hollweg, H.D., Ilyina, T., Kinne, S., Kornblueh, L., Matei, D., Mauritsen, T., Mikolajewicz, U., Mueller, W., Notz, D., Pithan, F., Raddatz, T., Rast, S., Redler, R., Roeckner, E., Schmidt, H., Schnur, R., Segschneider, J., Six, K.D., Stockhause, M., Timmreck, C., Wegner, J., Widmann, H., Wieners, K.H., Claussen, M., Marotzke, J., Stevens, B., 2013. Climate and carbon cycle changes from 1850 to 2100 in MPI-ESM simulations for the coupled model Intercomparison project phase 5. J. Adv. Model. Earth Syst. 5, 572–597. https://doi.org/10.1002/jame.20038.
Gobiet, A., Kotlarski, S., Beniston, M., Heinrich, G., Rajczak, J., Stoffel, M., 2014. 21st century climate change in the European Alps—a review. Sci. Total Environ. 493, 1138–1151. https://doi.org/10.1016/j.scitotenv.2013.07.050.
Goldscheider, N., 2019. A holistic approach to groundwater protection and ecosystem services in karst terrains. Carbonates Evaporites, 1–9 https://doi.org/10.4409/Am-046-12-0047.
Goldscheider, N., Chen, Z., Auler, A.S., Bakalowicz, M., Broda, S., Drew, D., Hartmann, H., Jiang, G., Moosdorf, N., Stevanovic, Z., Veni, G., 2020. Global distribution of carbonate rocks and karst water resources. Hydrogeol. J. https://doi.org/10.1007/s10040-020-02139-5.
González-Ramón, A., Jódar, J., Samsó, J.M. Martos-Rosillo, S., Heredia, J., Zabaleta, A., Antigüedad, I., Custodio, E., and Lambán, L.J. (2020). Hydrometeorological factors determining the development of water table cave patterns in alpine zones. The Ordesa and Monte Perdido National Park, NE-Spain. Int. J. Speleol. doi:https://doi.org/10.5038/1827-806X.49.3.2346.
Guan, J., Liu, Z., Wen, X., Brady, E., Noone, D., Zhu, J., and Han, J. (2016). Understanding the temporal slope of the temperature-water isotope relation during the deglaciation using isoCAM3: the slope equation. J. Geophys. Res. Atmos., 121, 10,342–10,354. doi:https://doi.org/10.1002/2016JD024955.
Hargreaves, G.H., Samani, Z.A., 1982. Estimating potential evapotranspiration. J. Irrig. Drain. Div. 108 (3), 225–230. https://doi.org/10.1061/JRCEA4.0001390.
Hartmann, A., Goldscheider, N., Wagener, T., Lange, J., Weiler, M., 2014. Karst water resources in a changing world: review of hydrological modeling approaches. Rev. Geophys. 52 (3), 218–242. https://doi.org/10.1002/2013RG000443.
Hartmann, A., Jasechko, S., Gleeson, T., Wada, Y., Andreo, B., Barberá, J.A., Brielmann, H., Bouchaou, L., Charlier, J.B., Darling, W.G., Filippini, M., Garvelmann, J., Goldscheider, N., Kralik, M., Kunstmann, H., Ladouche, B., Lange, J., Lucianetti, G., Martín, J.F., Mudarra, M., Sánchez, D., Stumpp, C., Zagana, E., Wagener, T., 2021. Risk of groundwater contamination widely underestimated because of fast flow into aquifers. Proc. Nat. Aca. Sci. 118 (20). https://doi.org/10.1073/pnas.2024492118.
Hay, L.E., Wilby, R.L., Leavesley, G.H., 2000. A comparison of delta change and downscaled GCM scenarios for three mountainous basins in the United States 1. JAWRA J. Am. Water Resour. Assoc. 36 (2), 387–397. https://doi.org/10.1111/j.1752-1688.2000.tb04276.x.
Helsel, D.R., Frans, L.M., 2006. Regional Kendall Test for trend. Environ. Sci. Technol. 40, 4066–4073. https://doi.org/10.1021/es051650b.
Helsel, D.R., Mueller, D.K., Slack, J.R., 2006. Computer Program for the Kendall Family of Trend Tests: U.S. Geological Survey Scientific Investigations Report 2005–5275 (4 p).
Henderson-Sellers, A., McGuffie, K., Noone, D., Irannejad, P., 2004. Using stable water isotopes to evaluate basin-scale simulations of surface water budgets. J. Hydrometeorol. 5 (5), 805–822. https://doi.org/10.1175/1525-7541(2004)005<0805:USWITE>2.0.CO;2.
Herms, I., Jódar, J., Soler, A., Vadillo, I., Lambán, L.J., Martos-Rosillo, S., Núñez, J.A., Arnó, G., Jorge, J., 2019. Contribution of isotopic research techniques to characterize high-mountain-Mediterranean karst aquifers: the Port del Comte (Eastern Pyrenees) aquifer. Sci. Total Environ. 656, 209–230. https://doi.org/10.1016/j.scitotenv.2018.11.188.
Herms, I., Jódar, J., Soler, A., Lambán, L.J., Custodio, E., Núñez, J.A., Arnó, G., Ortego, M.I., Parcerisa, D., Jorge, J., 2021. Evaluation of natural background levels of high mountain karst aquifers in complex hydrogeological settings. A Gaussian mixture model approach in the Port del Comte (SE, Pyrenees) case study. Sci. Total Environ. 756, 143864. https://doi.org/10.1016/j.scitotenv.2020.143864.
Hock, R., Rasul, G., Adler, C., Cáceres, B., Gruber, S., Hirabayashi, Y., Jackson, M., Kääb, A., Kang, S., Kutuzov, S., Milner, Al, Molau, U., Morin, S., Orlove, B., Steltzer, H., 2019. High mountain areas. In: Pörtner, H.O., Roberts, D.C., Masson-Delmotte, V., Zhai, P., Tignor, M., Poloczanska, E., Mintenbeck, K., Alegría, A., Nicolai, M., Okem, A., Petzold, J., Rama, B., Weyer, N.M. (Eds.), IPCC Special Report on the Ocean and Cryosphere in a Changing Climate Retrieved from. http://urn.kb.se/resolve?urn=urn:nbn:se:uu:diva-414230 (Last access 1/04/2021).
Hoerling, M., Eischeid, J., Perlwitz, J., Quan, X., Zhang, T., Pegion, P., 2012. On the increased frequency of Mediterranean drought. J. Clim. 25 (6), 2146–2161. https://doi.org/10.1175/JCLI-D-11-00296.1.
Hollander, M., Wolfe, D.A., 1973. Nonparametric Statistical Methods. John Wiley & Sons, New York.
Holloway, M.D., Sime, L.C., Singarayer, J.S., Tindall, J.C., Bunch, P., Valdes, P.J., 2016. Antarctic last interglacial isotope peak in response to sea ice retreat not ice-sheet collapse. Nat. Commun. 7, 12293. https://doi.org/10.1038/ncomms12293.
IPCC, 2019. Summary for policymakers. In: Pörtner, H.O., Roberts, D.C., Masson-Delmotte, V., Zhai, P., Tignor, M., Poloczanska, E., Mintenbeck, K., Alegría, A., Nicolai, M., Okem, A., Petzold, J., Rama, B., Weyer, N.M. (Eds.), IPCC Special Report on the Ocean and Cryosphere in a Changing Climate Retrieved from. http://urn.kb.se/resolve?urn=urn:nbn:se:uu:diva-414230 (Last access 1/04/2021, in press).
Jódar, J., Lambán, L.J., Medina, A., Custodio, E., 2014. Exact analytical solution of the convolution integral for classical hydrogeological lumped-parameter models and typical input tracer functions in natural gradient systems. J. Hydrol. 519, 3275–3289. https://doi.org/10.1016/j.jhydrol.2014.10.027.
Jódar, J., Custodio, E., Lambán, J.L., Martos-Rosillo, S., Herrera, C., Sapriza, G., 2016. Vertical variation in the amplitude of the seasonal isotopic content of rainfall as a tool to jointly estimate the groundwater recharge zone and transit times in the Ordesa and Monte Perdido National Park aquifer system, north-eastern Spain. Sci. Total Environ. https://doi.org/10.1016/j.scitotenv.2016.08.117.
Jódar, J., Carpintero, E., Martos-Rosillo, S., Ruiz-Constán, A., Marín-Lechado, C., Cabrera-Arrabal, J.A., Navarrete-Mazariegos, E., González-Ramón, A., Lambán, L.J., Herrera, C., González-Dugo, M.P., 2018. Combination of lumped hydrological and remote-sensing models to evaluate water resources in a semi-arid high altitude ungauged watershed of Sierra Nevada (Southern Spain). Sci. Total Environ. 625, 285–300. https://doi.org/10.1016/j.scitotenv.2017.12.300.
Jódar, J., González-Ramón, A., Martos-Rosillo, S., Heredia, J., Herrera, C., Urrutia, J., Caballero, Y., Zabaleta, A., Antigüedad, I., Custodio, E., Lambán, L.J., 2020. Snowmelt as a determinant factor in the hydrogeological behaviour of high mountain karst aquifers: the Garcés karst system, Central Pyrenees (Spain). Sci. Total Environ. https://doi.org/10.1016/j.scitotenv.2020.141363 (748-141363).
Kendall, M.G., 1975. Rank Correlation Methods. Griffin, London, UK.
Kiraly, L., 2003. Karstification and groundwater flow. In: Gabrovsek, F. (Ed.), Evolution of Karst: From Prekarst to Cessation. Zalozba ZRC, Postojna-Ljbljana, pp. 155–190.
Konz, M., Seibert, J., 2010. On the value of glacier mass balances for hydrological model calibration. J. Hydrol. 385 (1–4), 238–246. https://doi.org/10.1016/j.jhydrol.2010.02.025.
Lambert, S.J., Boer, G.J., 2001. CMIP1 evaluation and intercomparison of coupled climate models. Clim. Dyn. 17, 83–106. https://doi.org/10.1007/PL00013736.
Lauber, U., Goldscheider, N., 2014. Use of artificial and natural tracers to assess groundwater transit-time distribution and flow systems in a high-alpine karst system (Wetterstein Mountains, Germany). Hydrogeol. J. 22 (8), 1807–1824. https://doi.org/10.1007/s10040-014-1173-6.
Lohmann, G., Pfeiffer, M., Laepple, T., Leduc, G., Kim, J.H., 2013. A model–data comparison of the Holocene global sea surface temperature evolution. Clim. Past 9 (4), 1807–1839. https://doi.org/10.5194/cpd-8-1005-2012.
López-Moreno, J.I., García-Ruiz, J.M., 2004. Influence of snow accumulation and snowmelt on streamflow in the Central Spanish Pyrenees. Hydrol. Sci. J. 49 (5), 787–802. https://doi.org/10.1623/hysj.49.5.787.55135.
López-Moreno, J.I., Goyette, S., Beniston, M., 2008a. Climate change prediction over complex areas: spatial variability of uncertainties and predictions over the Pyrenees from a set of regional climate models. Int. J. Climatol. 28 (11), 1535–1550.
López-Moreno, J.I., Beniston, M., García-Ruiz, J.M., 2008b. Environmental change and water management in the Pyrenees: facts and future perspectives for Mediterranean mountains. Glob. Planet. Chang. 61 (3–4), 300–312. https://doi.org/10.1016/j.gloplacha.2007.10.004.
López-Moreno, J.I., Goyette, S., Beniston, M., 2009. Impact of climate change on snowpack in the Pyrenees: horizontal spatial variability and vertical gradients. J. Hydrol. 374 (3–4), 384–396. https://doi.org/10.1016/j.jhydrol.2009.06.049.
López-Moreno, J.I., Soubeyroux, J.M., Gascoin, S., Alonso-Gonzalez, E., Durán-Gómez, N., Lafaysse, M., Vernay, M., Carmagnola, C., Morin, S., 2020. Long-term trends (1958–2017) in snow cover duration and depth in the Pyrenees. Int. J. Climatol. 40, 6122–6136. https://doi.org/10.1002/joc.6571.
Mallucci, S., Majone, B., Bellin, A., 2019. Detection and attribution of hydrological changes in a large alpine river basin. J. Hydrol. 575, 1214–1229. https://doi.org/10.1016/j.jhydrol.2019.06.020.
Małoszewski, P., Zuber, A., 1996. Lumped parameter models for the interpretation of environmental tracer data. Manual on Mathematical Models in Isotope Hydrology. IAEA-TECDOC 910. IAEA, Vienna (Austria.

Małoszewski, P., Zuber, A., 2002. Manual on Lumped Parameter Models Used for the Interpretation of Environmental Tracer Data in Groundwaters (IAEA-UIAGS/CD-02-00131). International Atomic Energy Agency (IAEA) https://inis.iaea.org/search/search.aspx?orig_q=RN:33037906 (Last access 02/04/2021).

Małoszewski, P., Rauert, W., Trimborn, P., Herrmann, A., Rau, R., 1992. Isotope hydrological study of mean transit times in an alpine basin (Wimbachtal, Germany). J. Hydrol. 140, 343–360. https://doi.org/10.1016/0022-1694(92)90247-S.

Małoszewski, P., Stichler, W., Zuber, A., Rank, D., 2002. Identifying the flow systems in a karstic-fissured-porous aquifer, the Schneealpe, Austria, by modelling of environmental 18O and 3H isotopes. J. Hydrol. 256 (1–2), 48–59. https://doi.org/10.1016/S0022-1694(01)00526-1.

Mann, H.B., 1945. Nonparametric tests against trend. Econometrica 13 (3), 245–259. https://doi.org/10.2307/1907187.

Matiu, M., Crespi, A., Bertoldi, G., Carmagnola, C.M., Marty, C., Morin, S., Schöner, W., Cat Berro, D., Chiogna, G., De Gregorio, L., Kotlarski, S., Majone, B., Resch, G., Terzago, S., Valt, M., Beozzo, W., Cianfarra, P., Gouttevin, I., Marcolini, G., Notarnicola, C., Petitta, M., Scherrer, S.C., Strasser, U., Winkler, M., Zebisch, M., Cicogna, A., Cremonini, R., Debernardi, A., Faletto, M., Gaddo, M., Giovannini, L., Mercalli, L., Soubeyroux, J.M., Sušnik, A., Trenti, A., Urbani, S., Weilguni, V., 2021. Observed snow depth trends in the European Alps: 1971 to 2019. Cryosphere 15 (3), 1343–1382. https://doi.org/10.5194/tc-15-1343-2021.

Meeks, J., Hunkeler, D., 2015. Snowmelt infiltration and storage within a karstic environment, Vers Chez le Brandt, Switzerland. J. Hydrol. 529, 11–21. https://doi.org/10.1016/j.jhydrol.2015.06.040.

Moss, R.H., Edmonds, J.A., Hibbard, K.A., Manning, M.R., Rose, S.K., Van Vuuren, D.P., Carter, T.R., Emori, S., Kainuma, M., Kram, T., Meehl, G.A., Mitchell, J.F.B., Nakicenovic, N., Riahi, K., Smith, S.J., Stouffer, R.J., Thomson, A.M., Weyant, J.P., Wilbanks, T.J., 2010. The next generation of scenarios for climate change research and assessment. Nature 463, 747–756. https://doi.org/10.1038/nature08823.

Motyka, J.A., 1998. Conceptual model of hydraulic networks in carbonate rocks, illustrated by examples from Poland. Hydrogeol. J. 6, 469–482. https://doi.org/10.1007/s100400050169.

Müller, M.H., Weingartner, R., Alewell, C., 2013. Importance of vegetation, topography and flow paths for water transit times of base flow in alpine headwater catchments. Hydrol. Earth Syst. Sci. 17 (4), 1661–1679. https://doi.org/10.5194/hess-17-1661-2013.

Okazaki, A., Yoshimura, K., 2019. Global evaluation of proxy system models for stable water isotopes with realistic atmospheric forcing. J. Geophys. Res. Atmos. 124 (16), 8972–8993. https://doi.org/10.1029/2018JD029463.

Parise, M., Closson, D., Gutiérrez, F., Stevanović, Z., 2015. Anticipating and managing engineering problems in the complex karst environment. Environ. Earth Sci. 74, 7823–7835. https://doi.org/10.1007/s12665-015-4647-5.

Pedro-Monzonís, M., Solera, A., Ferrer, J., Estrela, T., Paredes-Arquiola, J., 2015. A review of water scarcity and drought indexes in water resources planning and management. J. Hydrol. 527, 482–493. https://doi.org/10.1016/j.jhydrol.2015.05.003.

Pfeiffer, M., Lohmann, G., 2016. Greenland ice sheet influence on last interglacial climate: global sensitivity studies performed with an atmosphere–ocean general circulation model. Clim. Past 12 (6), 1313–1338. https://doi.org/10.5194/cpd-11-933-2015.

Räty, O., Räisänen, J., Ylhäisi, J.S., 2014. Evaluation of delta change and bias correction methods for future daily precipitation: intermodel cross-validation using ENSEMBLES simulations. Clim. Dyn. 42 (9–10), 2287–2303. https://doi.org/10.1007/s00382-014-2130-8.

Rowley, D.B., Garzione, C.N., 2007. Stable isotope-based paleoaltimetry. Annu. Rev. Earth Planet. Sci. 35, 463–508. https://doi.org/10.1146/annurev.earth.35.031306.140155.

Rozanski, K., Araguas-Araguas, L., Gonfiantini, R., 1992. Relation between long-term trends of oxygen-18 isotope composition of precipitation and climate. Science 258 (5084), 981–985. https://doi.org/10.1126/science.258.5084.981.

Schmidt, G.A., Annan, J.D., Bartlein, P.J., Cook, B.I., Guilyardi, E., Hargreaves, J.C., Harrison, S.P., Kageyama, M., LeGrande, A.N., Konecky, B., Lovejoy, S., Mann, M.E., Masson-Delmotte, V., Risi, C., Thompson, D., Timmermann, A., Tremblay, L.-B., Yiou, P., 2014. Using palaeo-climate comparisons to constrain future projections in CMIP5. Clim. Past 10, 221–250. https://doi.org/10.5194/cp-10-221-2014.

Seibert, J., Vis, M.J.P., 2012. Teaching hydrological modelling with a user-friendly catchment-runoff-model software package. Hydrol. Earth Syst. Sci. 16 (9), 3315–3325. https://doi.org/10.5194/hess-16-3315-2012 (102012).

Sen, P.K., 1968. Estimates of the regression coefficient based on Kendall's Tau. J. Am. Stat. Assoc. 63 (324), 1379–1389. https://doi.org/10.1080/01621459.1968.10480934.

Sjolte, J., Hoffmann, G., 2014. Modelling stable water isotopes in monsoon precipitation during the previous interglacial. Quat. Sci. Rev. 85, 119–135. https://doi.org/10.1016/j.quascirev.2013.12.006.

Sjolte, J., Adolphi, F., Vinther, B.M., Muscheler, R., Sturm, C., Werner, M., Lohmann, G., 2020. Seasonal reconstructions coupling ice core data and an isotope-enabled climate model–methodological implications of seasonality, climate modes and selection of proxy data. Clim. Past 16 (5), 1737–1758. https://doi.org/10.5194/cp-2019-72.

Staudinger, M., Stoelzle, M., Seeger, S., Seibert, J., Weiler, M., Stahl, K., 2017. Catchment water storage variation with elevation. Hydrol. Process. 31 (11), 2000–2015. https://doi.org/10.1002/hyp.11158.

Taylor, K.E., Stouffer, R.J., Meehl, G.A., 2012. An overview of CMIP5 and the experiment design. Bull. Am. Meteorol. Soc. 93, 485–498. https://doi.org/10.1175/BAMS-D-11–00094.1.

Van Vuuren, D.P., Edmonds, J., Kainuma, M., Riahi, K., Thomson, A., Hibbard, K., Hurtt, G.C., Kram, T., Krey, V., Lamarque, J.F., Masui, T., Meinshausen, M., Nakicenovic, N., Smith, S.J., Rose, S.K., 2011. The representative concentration pathways: an overview. Clim. Chang. 109 (1), 5–31. https://doi.org/10.1007/s10584-011-0148-z.

Vicente-Serrano, S.M., López-Moreno, J.I., Beguería, S., Lorenzo-Lacruz, J., Sanchez-Lorenzo, A., García-Ruiz, J.M., Azorin-Molina, C., Morán-Tejeda, E., Revuelto, J., Trigo, R., Coelho, F., Espejo, F., 2014. Evidence of increasing drought severity caused by temperature rise in southern Europe. Environ. Res. Lett. 9 (4), 044001. https://doi.org/10.1088/1748-9326/9/4/044001.

Viviroli, D., Dür, H.H., Messerli, B., Meybeck, M., Weingartner, R., 2007. Mountains of the world, water towers for humanity: topology, mapping and global significance. Water Resour. Res. 43, W07447. https://doi.org/10.1029/2006WR005653.

Voldoire, A., Sánchez-Gómez, E., Salas y Mélia, D., Decharme, B., Cassou, C., Sénési, S., Valcke, S., Beau, I., Alias, A., Chevallier, M., Déqué, M., Deshayes, J., Douville, H., Fernández, E., Madec, G., Maisonnave, E., Moine, M.P., Planton, S., Saint-Martin, D., Szopa, S., Tyteca, S., Alkama, R., Belamari, S., Braun, A., Coquart, L., Chauvin, F., 2013. The CNRM-CM5. 1 global climate model: description and basic evaluation. Clim. Dyn. 40 (9), 2091–2121. https://doi.org/10.1007/s00382-011-1259-y.

Volodin, E.M., Dianskii, N.A., Gusev, A.V., 2010. Simulating present-day climate with the INMCM4. 0 coupled model of the atmospheric and oceanic general circulations. Izvestiya Atmos. Ocean. Phys. 46 (4), 414–431. https://doi.org/10.1134/S000143381004002X.

Wassenaar, L.I., Terzer-Wassmuth, S., Douence, C., Araguas-Araguas, L., Aggarwal, P.K., Coplen, T.B., 2018. Seeking excellence: an evaluation of 235 international laboratories conducting water isotope analyses by isotope-ratio and laser-absorption spectrometry. Rapid Commun. Mass Spectrom. 32 (5), 393–406. https://doi.org/10.1002/rcm.6270.

Watanabe, S., Hajima, T., Sudo, K., Nagashima, T., Takemura, T., Okajima, H., Nozawa, T., Kawase, H., Abe, M., Yokohata, T., Ise, T., Sato, H., Kato, E., Takata, K., Emori, S., Kawamiya, M., 2011. MIROC-ESM 2010: model description and basic results of CMIP5-20c3m experiments. Geosci. Model Dev. 4 (4), 845. https://doi.org/10.5194/gmd-4-845-2011.

Wu, T., Song, L., Li, W., Wang, Z., Zhang, H., Xin, X., Zhang, Y., Zhang, L., Li, J., Wu, F., Liu, Y., Zhang, F., Shi, X., Chu, M., Zhang, J., Fang, Y., Wang, F., Lu, Y., Liu, X., Wei, M., Liu, Q., Zhou, W., Dong, M., Zhao, Q., Ji, J., Laurent, L., Zhou, M., 2014. An overview of BCC climate system model development and application for climate change studies. J. Meteorol. Res. 28 (1), 34–56. https://doi.org/10.1007/s13351-014-3041-7.

Yoshimura, K., 2015. Stable water isotopes in climatology, meteorology, and hydrology: a review. J. Meteorol. Soc. Japan. Ser. II, 93 (5), 513–533. https://doi.org/10.2151/jmsj.2015-036.

Yukimoto, S., Adachi, Y., Hosaka, M., Sakami, T., Yoshimura, H., Hirabara, M., Tanaka, T.Y., Shindo, E., Tsujino, H., Deushi, M., Mizuta, R., Yabu, S., Obata, A., Nakano, H., Koshiro, T., Ose, T., Kitoh, A., 2012. A new global climate model of the meteorological research institute: MRI-CGCM3—model description and basic performance—. J. Meteorol. Soc. Japan. Ser. II, 90, 23–64. https://doi.org/10.2151/jmsj.2012-A02.

Zaiontz, C., 2020. Real Statistics Using Excel. www.real-statistics.com (Last access 01/01/2021).

Zuber, A., 1986. Mathematical models for the interpretation of environmental radioisotopes in groundwater systems. Handbook of Environmental Isotope Geochemistry, Terrestrial Environment, pp. 1–59.